Magnetic structures and magnetic anisotropy of $Mn_{3-x}Fe_xSn$ studied by first-principles calculations

Katsunori Tagami[1,2*], Takahisa Ohno[2], Jun Nara[2], and Mamoru Usami[1]

[1] *ASMS Co., Ltd., Shinagawa, Tokyo 141-0022, Japan*

2 National Institute for Materials Science (NIMS), Tsukuba, Ibaraki 305-0044, Japan

Abstract

Aiming at clarifying the structures and magnetic anisotropies of kagome $Mn_{3-x}Fe_xSn$ crystal over the wide range of x, we theoretically investigate the x-dependence of lattice parameters and bond lengths of their six magnetic phases by the first-principles calculations, and discuss their stabilities. Under the virtual crystal approximation at the Mn/Fe sites with a composition increment of $\Delta x=0.25$, we find the following points. First, the lattice parameters and intra-plane first-neighbor bond lengths highly depend on the magnetic structures. Second, at $x \leq 0.25$, the in-plane noncollinear antiferromagnetic phase is most stable. Third, at x=0.50, magnetic structures such as the out-of-plane spin canting structure, which are like superpositions of the antiferromagnetic and ferromagnetic phases, are stable, and the magnetization easy axis is the c-axis. Finally, at $x \geq 1.00$, the in-plane ferromagnetic phase is most stable, indicating that the easy axis is in the ab-plane, and the magnetocrystalline anisotropy energy reaches -1.60 MJ/m^3 at x=3.00.

*E-mail: ktagami@asms.co.jp

1. Introduction

So far, plenty of researches have been performed for tuning magnetic properties such as the Curie temperature (Tc) and the magnetocrystalline anisotropy energy (MAE) of magnetic materials by chemical doping. Among them, substituting Fe atoms for the Mn sites in the Mn_3Sn crystal, which has a hexagonal crystal structure with a space group $P6_3/mmc$, exhibits various magnetic structures depending on the Fe concentration. At x=0.00 of $Mn_{3-x}Fe_xSn$, the magnetic moments at the Mn sites of Mn_3Sn form a noncollinear in-plane antiferromagnetic (IAFM) structure below the Néel temperature of 420 K[1)], in which the in-plane Mn magnetic moments show the chiral 120° inverse triangular structure[1)-3)]. At x=3.00, on the other hand, Fe_3Sn is a ferromagnet below Tc of 725 K, and its easy magnetization axis lies in the ab plane[4)]. The experimentally measured MAE density amounts to -1.8 MJ/m^3 [4)] or -1.0 MJ/m^3 [5)] at room temperature. Here, the MAE is defined by the energy of the in-plane ferromagnetic (IFM) phase with respect to the energy of the out-of-plane ferromagnetic (OFM) phase. Between the two limits of x=0.00 and x=3.00, complicated magnetic features have been reported[6)-9)]. For example, at x=0.58[7)], x=0.90[8)], and x=1.10[9)], by the measurement of temperature dependence of magnetization under external magnetic field, it has been understood that the ferromagnetic (FM) and antiferromagnetic (AFM) phases coexist at low temperatures[10)]. Moreover, at x=0.35[11)] and x=0.58[7)], the MAEs are 0.53 MJ/m^3 and 0.47 MJ/m^3 [12)], respectively, indicating that the easy magnetization axis is the c-axis. As x is increased up to 1.50 and 10% of Sn is substituted by Sb, i.e., $Mn_{1.5}Fe_{1.5}Sn_{0.9}Sb_{0.1}$[4)], the easy axis is now in the ab-plane, although the MAE is smaller than that of Fe_3Sn.

Compared to these experimental studies, not many theoretical calculations of $Mn_{3-x}Fe_xSn$ ($0.00<x<3.00$) have been performed. At x=0.50 and x=0.75, the noncoplanar magnetic structure is predicted to emerge, in which the Mn magnetic moments cant from the ab-plane[13)]. At x=2.25, the negative MAE is predicted[4)], indicating that the easy axis is in the ab-plane. However, it has not been clear how the structures, such as lattice constants and bond lengths, and the MAEs change over the wide range of x. Under these circumstances, comprehensive theoretical researches of $Mn_{3-x}Fe_xSn$ are desired.

In this work, as a first step for deeper understanding of the structural and magnetic properties of $Mn_{3-x}Fe_xSn$ ($0.00\leq x\leq 3.00$) theoretically, we optimize the lattice parameters and fractional coordinates of six magnetic phases (IFM, OFM, IAFM, and their mixed models) with a composition increment of $\Delta x=0.25$ by the first-principles density functional theory (DFT) calculations, and investigate their stabilities. For the treatment of disorder at the Mn/Fe sites, we adopt the virtual crystal approximation (VCA) [14)-16)],

which have been applied to various materials in the literature.

We find the following points. (1) The lattice parameters and intra-plane first-neighbor bond lengths highly depend on the magnetic structures. (2) At $x \leq 0.25$, the IAFM is most stable. (3) At x=0.50, the out-of-plane spin canting (OSC) model and the in-plane spin rotation (ISR) model, which are like the superpositions of the FM and IAFM phases, are more stable than the IFM and OFM phases. This suggests that the OSC and ISR magnetic structures can exist in a single domain, or that they are spatially averaged magnetic structures which can include the FM (OFM or IFM) and IAFM domains. The MAE between the IFM and OFM phases is 0.37 MJ/m^3, indicating the easy axis is the c-axis. (4) At $x \geq 1.00$, the IFM phase is most stable and the easy axis is in the ab-plane. The MAE reaches -1.60 MJ/m^3 at x=3.00, which agrees well with previous theoretical studies.

The rest of this article is organized as follows. In Sec. 2 the details of theoretical methods are described. In Sec. 3 the results are presented and are discussed. In Sec. 4 the article is concluded. In Appendix the results using the special quasirandom structure (SQS) models are presented in order to show the validity of VCA.

2. Theoretical methods

In this work, we assume six magnetic structures as illustrated in Fig. 1, where the primitive cell of $Mn_{3-x}Fe_xSn$ is shown. The brown and gray spheres correspond to the Mn/Fe and Sn atoms, respectively. In the VCA[14)-16)] approach, all the Mn/Fe atoms are treated as $Mn_{1-x/3}Fe_{x/3}$ which has a nuclear charges of 25+x/3. The arrows in Fig. 1 indicate the orientation of the spin magnetic moments considered in this study, i.e., (a) OFM, (b) IFM, (c) IAFM, (d) out-of-plane antiferromagnetic (OAFM) phases, and (e), (f) their mixed magnetic structures. In the (e) OSC model, θ is a canting angle measured from the ab plane, and the configurations with θ=90° and 0° are equivalent to the (a) OFM and (c) IAFM phases, respectively. In the (f) ISR model, ϕ is a spin rotation angle at the chosen sites, and the configurations with ϕ=0° and 120° are equivalent to the (b) IFM and (c) IAFM phases, respectively.

The DFT calculations are performed using a software PHASE/0[17)], in which the Kohn-Sham equations are solved self-consistently by the planewave basis set combined with the projected augmented wave (PAW) pseudopotential method[18),19)]. The planewave cutoff energies of the wavefunctions and charge densities are 50 and 300 Rydberg, respectively. The exchange correlation functional is GGA-PBE[20)]. The $Mn_{1-x/3}Fe_{x/3}$ (3d,4s) and Sn(4d,5s,5p) electrons are treated as valence, and the corresponding

pseudopotentials are generated by using a software CIAO[21].

In the optimization of the lattice parameters and internal coordinates, the spin-orbit interaction (SOI) is incorporated in the self-consistent manner using the two-component spinor wavefunctions[22)-24)], and a 6×6×8 shifted Monkhorst-Pack k-point mesh is used. The electronic, force, and stress convergence criteria are set to 10^{-8} Hartree/atom, 2×10^{-4} Hartree/Bohr, and 10^{-6} Hartree/Bohr^3, respectively. In the OSC and ISR models, for each value of x, we set the initial spin angles at θ=30° and ϕ=70°, respectively.

In calculating the MAE between the two FM phases, i.e., IFM and OFM, the SOI is included by the second variational method[25)], and a 32×32×40 Γ-centered k-point mesh is used. In this method, the SOI is applied to the wavefunctions which are obtained beforehand without SOI, and the electronic states are not solved in the self-consistent manner. Here, the lattice parameters and internal coordinates are fixed at their optimized values for the lower energy state between the IFM and OFM phases, which are obtained as in the previous paragraph.

3. Results and discussion

3.1 structural parameters

In Table I, the optimized lattice parameters of kagome Mn_3Sn and Fe_3Sn crystals are shown, where they are assumed to be at the magnetic ground state at the ambient conditions, i.e., IAFM (Mn_3Sn) and IFM (Fe_3Sn) phases. It is found that both the in-plane (a_0) and out-of-plane (c_0) lattice parameters in Fe_3Sn are smaller than those of Mn_3Sn, which agrees well with experiments[5),26)].

Figures 2(a) and 2(b) show the lattice parameters of the IFM (blue solid squares), IAFM (black solid circles), OAFM (black open circles), OSC (red solid triangles), and ISR (red open triangles) structures for each value of x. As the lattice parameters of the OFM phase do not differ from those of the IFM phase, they are not shown in the figure. As a whole, the lattice parameters highly depend on the magnetic phases of $Mn_{3-x}Fe_xSn$. In the IFM phase, a_0 and c_0 slightly change as a function of x, and range from 5.436 to 5.465 Å, and from 4.279 to 4.343 Å, respectively. In the IAFM phase, both a_0 and c_0 decrease monotonically against x. In the OSC and ISR phases, both a_0 and c_0 change dramatically at $0.25<x<1.25$, and they take similar values to those of the IAFM (IFM) phase at $x\leq0.25$ ($x\geq1.25$). In the OAFM phase, except c_0 at $x<0.75$, a_0 (c_0) is shorter (longer) than those values in the other magnetic phases.

In Fig. 3, the intra-plane first-neighbor bond lengths of these magnetic structures are

plotted for the IFM (blue solid squares), IAFM (black solid circles), OAFM (black open circles), OSC (red solid triangles), and ISR (red open triangles) structures. It is found that the bond lengths in the FM phases are shorter than those values in the AFM phases, except in the OAFM phase at x≥2.25. From Figs. 2 and 3, at x≥1.25, the structural parameters of the OSC and ISR models are very close to the IFM phases, which indicates that the OSC (ISR) is basically identical to the OFM (IFM) phase. At x≤0.25, in a similar manner, the OSC and ISR is identical to the IAFM phase.

3.2 spin magnetic moments

Figure 4 shows the atomic spin magnetic moments (M_{atom}) of the IFM (blue solid squares), IAFM (black solid circles), OAFM (black open circles), OSC (red solid triangles), and ISR (red open triangles) structures. Here, M_{atom} is estimated in the following way. First, the local moment vector $\mathbf{M}_i$ is calculated by integrating the spin magnetic density within a certain cutoff radius r_{cut} from each $Mn_{1-x/3}Fe_{x/3}$ site. Then, the absolute values of $\mathbf{M}_i$ are averaged over the six sites in the primitive cell. The values of r_{cut} are set to 1.16 Å (x=3.00) and 1.19 Å (otherwise), which correspond to the covalent radii[27] of Fe and Mn atoms, respectively. As M_{atom} of the OFM phase does not differ from those of IFM phase, it is not shown in the figure. In the IFM phase, M_{atom} is found to jump from 1.86 (x=1.25) to 2.34 μ_B(x=1.75), and to reach 2.38 μ_B at x=3.00, which agrees well with those values in the previous DFT studies of Fe_3Sn, 2.41[4] or 2.31[5] μ_B. In the IAFM phase, M_{atom} is 2.86 μ_B at x=0.00, which is close to the experimentally measured value ($\sim 3.0\mu_B$)[28], and it decreases monotonically to 1.97 μ_B (x=3.00). In the OSC and ISR phases, M_{atom} decreases monotonically at 0.25<x<1.25, and takes similar values to those of the IAFM (IFM) phase at x≤0.25 (x≥1.25).

In Fig. 5, the canting angle θ and rotation angle ϕ of the OSC (solid circles) and ISR (open circles) models are plotted, which are obtained from the orientation of $\mathbf{M}_i$. At x≤0.25 (x≥1.25), θ is close to 0° (90°), indicating that the OSC model is almost identical to the IAFM (OFM) phase. In a similar manner, at x≤0.25 (x≥1.25), ϕ is close to 120° (0°), and the OSC model is identical to the IAFM (IFM) phase. The angles θ=33° (x=0.50) and 40° (x=0.75) are close to the values reported in a previous DFT study[13], 23° (x=0.50) and 37° (x=0.75), respectively.

Finally, we comment on the total spin magnetic moments M_{tot} (not shown). M_{tot} of the IFM phase is 5.22 μ_B per formula unit (f.u.) at x=0.00, then jumps from 5.51 (x=1.25) to 6.86 μ_B/f.u. (x=1.75), and reaches 6.98 μ_B/f.u. at x=3.00. At x=0.50, M_{tot} of the OSC and

ISR models are 4.32 and 4.19 μ_B/f.u., which are 81% and 78% of the corresponding value of the IFM phase. At x=1.00, M_{tot} of these two models are close to the value of IFM phase, 5.42 μ_B/f.u.

3.3 energy differences

Figure 6 shows the energy differences (ΔE_{tot}) of the magnetic structures, which are calculated by the PAW total energy (E_{tot}) of the IFM (blue solid squares), IAFM (black solid circles), OAFM (black open circles), OSC (red solid triangles), and ISR (red open triangles) structures, with respect to E_{tot}(OFM). It is found that the lowest energy state is the IAFM ($x \leq 0.25$), OSC or ISR (x=0.50), IFM or OFM ($x \geq 0.75$) structure. At x=0.50, ΔE_{tot}(OSC) and ΔE_{tot}(ISR) are -34 and -37 meV/f.u., respectively. At x=0.75, both of ΔE_{tot}(OSC) and ΔE_{tot}(ISR) are only 2 meV/f.u.. Then, at x=1.00, ΔE_{tot}(OSC) and ΔE_{tot}(ISR) are 24 and 20 meV/f.u., respectively, which indicates that the OSC and ISR magnetic structures are the metastable ones. These two structures at x=1.00 lie in the shallow minima in the energy-volume curves, and they easily change into the OFM and IFM phases by a weak hydrostatic pressure of about 2 GPa.

As in the above, we found that at $0.50 \leq x \leq 1.00$ the OSC and ISR magnetic structures, which are like the superpositions of FM and IAFM phases, are stable or metastable. However, this does not exclude a possibility of phase separation in which the FM (OFM or IFM) and IAFM domains coexist at the ground state[7)-9)]. Our calculations are based on the VCA, in which all the Mn/Fe atoms are replaced equally by the virtual atoms $Mn_{1-x/3}Fe_{x/3}$ which have an averaged atomic potential between Mn and Fe elements. This means that effects of nonuniformity of the local Fe concentration are neglected. If the Fe concentration varies locally in the samples, it is reasonable to expect that the IAFM domains appear at the region with nearly zero Fe concentration while the FM (OFM or IFM) domains appear at the region with high Fe concentration. In such cases, the OSC or ISR magnetic models are considered as the spatially averaged magnetic structures.

Finally, in order to achieve the energy difference between the IFM and OFM phases, i.e., the so-called MAE, more accurately, we use the second variational method with finer k-point grids, as denoted in the previous section. Although the MAE can be also calculated by the self-consistent calculations with the SOI, the computational cost is very high when the number of k-points is large. Here, the MAE is estimated by the difference of the band energy (E_{band}) between the IFM and OFM phases, i.e., E_{band}(IFM) - E_{band}(OFM). Figure 7 shows the MAEs plotted against x. At x=0.50 and 0.75, the MAEs

are 3 meV/f.u. (0.37 MJ/m^3) and 0.08 meV/f.u. (0.24 MJ/m^3), respectively, which indicates that magnetization easy axis is the c-axis. This point agrees with the experimentally observed out-of-plane magnetic anisotropy at x=0.35[11] and x=0.58[7]. At x≥1.00, the MAEs turn to be negative and the IFM phase is most stable. At x=3.00, the MAE reaches -0.56 meV/f.u. (-1.60 MJ/m^3), which is close to the values by the previous DFT studies of Fe_3Sn, -1.59 MJ/m^3 [4] and -1.62 MJ/m^3 [5].

4. Conclusions

In summary, aiming at clarifying the structures and magnetic anisotropies of kagome $Mn_{3-x}Fe_xSn$ crystal over the wide range of x, which have not been studied sufficiently, we investigated the x-dependence of lattice parameters and bond lengths of their six magnetic phases by the DFT calculations within the VCA, and discussed their stabilities. We found the following points. (1) The lattice parameters and intra-plane first-neighbor bond lengths highly depend on the magnetic structures. (2) At x≤0.25, the IAFM is most stable. (3) At x=0.50, the OSC and ISR models are more stable than the IFM and OFM phases. This suggests that the OSC and ISR magnetic structures can exist in a single domain, or that they are spatially averaged magnetic structures which can include the FM (OFM or IFM) and IAFM domains. The MAE between the IFM and OFM phases is 0.13 meV/f.u. (0.37 MJ/m^3), indicating the easy axis is the c-axis. (4) At x≥1.00, the IFM phase is most stable and the easy axis is in the ab-plane. The MAE reaches -0.56 meV/f.u. (-1.60 MJ/m^3) at x=3.00, which agrees well with previous theoretical studies.

Acknowledgements

The calculations were performed on the Numerical Materials Simulator of NIMS. The atomic models were illustrated by using a software VESTA[29].

Appendix

Here, we introduce the results of calculations performed without the VCA (see supplementary data). We adopt the supercell models which contain $2\times2\times2$ primitive cells, in which the Mn and Fe positions are determined by the SQS method[30]. The lattice parameters are fixed at the values obtained with the VCA method shown in Fig. 2. In the optimization of the internal coordinates, the spin-polarized DFT is used and the SOI is neglected. Thus, the spin orientation of Mn/Fe sites cannot be defined in this method, but their spin polarization is still well described. The planewave cutoff energies of the wavefunctions and charge densities are 30 and 270 Rydberg, respectively. The 3×3×4 shifted Monkhorst-Pack k-point mesh is used, and the electronic, force convergence criteria are set to 10^{-8} Hartree/atom, 2×10^{-4} Hartree/Bohr, respectively.

Figure S1 illustrates an example of the SQS model for the AFM phase (x=1.00), which mimics the OAFM phase (Fig. 1(d)). The brown, green, and gray spheres correspond to the Mn, Fe, and Sn atoms, respectively. The blue arrows indicate the spin polarization at each layer. In the FM phase, the spin polarization at every layer is aligned in parallel.

Figure S2 shows M_{atom} of the FM (blue solid squares) and AFM (black open circles) phases for each value of x. The error bars indicate the minima and maxima of M_{atom}, while the symbols correspond to the averaged values of M_{atom}, i.e., $\langle M_{atom}\rangle$. It is found that M_{atom} at the Mn/Fe sites takes various values, which reflect that the local (Mn-Mn, Mn-Fe, Fe-Fe) bonding configurations differ site by site. In addition, at x>1.75, the values of $\langle M_{atom}\rangle$ of the FM phase are found to be larger than those of the AFM phase, which agrees well with the result obtained by the VCA (Fig. 4).

Figure S3 shows the energy differences (ΔE_{tot}) of the two magnetic phases, which are calculated by the PAW total energy (E_{tot}) of the AFM with respect to E_{tot}(FM). It is found that ΔE_{tot} increases monotonically against x, and that the two phases are energetically comparable at x=0.50. These features are also observed in the calculations by the VCA (Fig. 6), indicating the validity of the VCA method adopted in this work.

References

1) S. Tomiyoshi and Y. Yamaguchi, J. Phys. Soc. Jpn. **51**, 2478 (1982).
2) S. Nakatsuji, N. Kiyohara, and T. Higo, Nature **527**, 212 (2015).
3) P. J. Brown, V. Nunez, F. Tasset, J. B. Forsyth, and P. Radhakrishna, J. Phys. Condens. Matter **2**, 9409 (1990).
4) B. C. Sales. B. Saparov, M. A. Saparov, D. J. Singh, and D. S. Parker, Sci. Reports **4**, 7024 (2014).
5) L. Prodan, D. M. Evans, S. M. Griffin, A. Östlin, M. Altthaler, E. Lysne, I. G. . Filippova, S. Shova, L. Chioncel, V. Tsurkan, and I. Kézsmárki, Appl. Phys. Lett. **123**, 021901 (2023).
6) M. R. Felez, A. A. Coelho, and S. Gama, J. Magn. Magn. Mater. **444**, 280 (2017).
7) W. Shen, Y. Huang, X. Yao, F. Qi, and G. Cao, J. Alloy. Compd. **970**, 172468 (2024).
8) J. Liu, S. Zuo, H. Li, Y. Liu, X. Zheng, Y. Zhang, T. Zhao, F. Hu, J. Sun, and B. Shen, Scr. Mater. **187**, 268 (2020).
9) J. Liu, S. Zuo, X. Zheng, Y. Zhang, T. Zhao, F. Hu, J. Sun, and B. Shen, Appl. Phys. Lett. **117**, 052407 (2020).
10) T. Hori, H. Niida, Y, Yamaguchi, H, Kato, and Y. Nakagawa, J. Magn. Magn. Mater. **90-91**, 159 (1990).
11) A. Low, S. Ghosh, S. Changdar, S. Routh, S. Purwar, and S. Thirupathaiah, Phys. Rev. B **106**, 144429 (2022).
12) Summation of K_1 and K_2 in ref. 7).
13) C. Singh, S. Jamaluddin, A. K. Nandy, M. Tokunaga, M. Avdeev, and A. K. Nayak, arXiv:2211.12722 (2022).
14) L. Boeri, J. Kortus, and K. Andersen, Phys. Rev. Lett. **93**, 237002 (2004).

15) K. W. Lee and W. E. Pickett, Phys. Rev. Lett. **93**, 237003 (2004).

16) K. Tagami, J. Koga, Y. Nohara, and M. Usami, Jpn. J. Appl. Phys. **56**, 058004 (2017).

17) T. Yamasaki, A. Kuroda, T. Kato, J. Nara, J. Koga, T. Uda, K. Minami, and T. Ohno, Comput. Phys. Commun. **244**, 264 (2019).

18) P. E. Blöchl, Phys. Rev. B **50**, 17953 (1994).

19) G. Kresse and D. Joubert, Phys. Rev. B **59**, 1758 (1999).

20) J. P. Perdew, K. Burke, and M. Ernzerhof, Phys. Rev. Lett. **77**, 3865 (1996).

21) https://azuma.nims.go.jp/software/ciao

22) S. Steiner, S. Khmelevskyi, M. Marsmann, and G. Kresse, Phys. Rev. B **93**, 224425 (2016).

23) Y. Miura and K. Masuda, Phys. Rev. Materials **5**, L101402 (2021).

24) S. A. Putri, Y. Yamaguchi, T. A. Ariasoca, M. Y. H. Widianto, K. Tagami, and M. Saito, Surf. Sci. **714**, 121917 (2021).

25) D. D. Koelling and B. N. Harmon, J. Phys. C: Solid State Phys. **10** 3107 (1977).

26) S. Tomiyoshi, J. Phys. Soc. Jpn., **51**, 803 (1982).

27) P. Pyykkö and M. Atsumi, Chem. Eur. J. **15**, 186 (2009).

28) P. J. Brown, V. Nunez, F. Tasset, J. B. Forsyth, and P. Radhakrishna, J. Phys.: Condens. Matter **2**, 9409 (1990).

29) K. Momma and F. Izumi, J. Appl. Crystallogr., **44**, 1272 (2011).

30) A. van de Walle, P. Tiwary, M. de Jong, D. L. Olmsted, M. Asta, A. Dick, D. Shin, Y. Wang, L. -Q. Chen, and Z. -K. Liu, Calphad **42**, 13 (2013).

Figure Captions

Fig. 1. (Color Online) Crystal and magnetic structures of $Mn_{3-x}Fe_xSn$ considered, (a) OFM, (b) IFM, (c) IAFM, (d) OAFM phases, (e) OSC, and (f) ISR models. The arrows indicate the orientation of the spin magnetic moments. The brown and gray spheres correspond to the Mn/Fe and Sn atoms, respectively.

Fig. 2. (Color Online) (a) In-plane and (b) out-of-plane lattice parameters of IFM (blue solid squares), IAFM (black solid circles), OAFM (black open circles), OSC (red triangles), and ISR (red open triangles) structures.

Fig. 3. (Color Online) Intra-plane bond lengths of IFM (blue solid squares), IAFM (black solid circles), OAFM (black open circles), OSC (red solid triangles), and ISR (red open triangles) structures.

Fig. 4. (Color Online) Atomic spin magnetic moments of IFM (blue solid squares), IAFM (black solid circles), OAFM (black open circles), OSC (red solid triangles), and ISR (red open triangles) structures.

Fig. 5. Spin canting angle of OSC (solid circles) and spin rotation angle of ISR (open circles) magnetic structures.

Fig. 6. (Color Online) Total energies of IFM (blue solid squares), IAFM (black solid circles), OAFM (black open circles), OSC (red solid triangles), and ISR (red open triangles) structures with respect to the total energy of the OFM phase.

Fig. 7. MAE between IFM and OFM phases.

Table I. Calculated lattice parameters and intra-plane first-neighbor bond lengths of Mn_3Sn and Fe_3Sn. The values in parentheses correspond to the experiments.

system	magnetic phase	a_0 (Å)	c_0 (Å)	bond length (Å)
Mn_3Sn[26]	IAFM	5.563	4.433	2.640
		(5.665)	(4.531)	(2.740)
Fe_3Sn[5]	IFM	5.465	4.325	2.470
		(5.4604)	(4.3458)	(2.529)

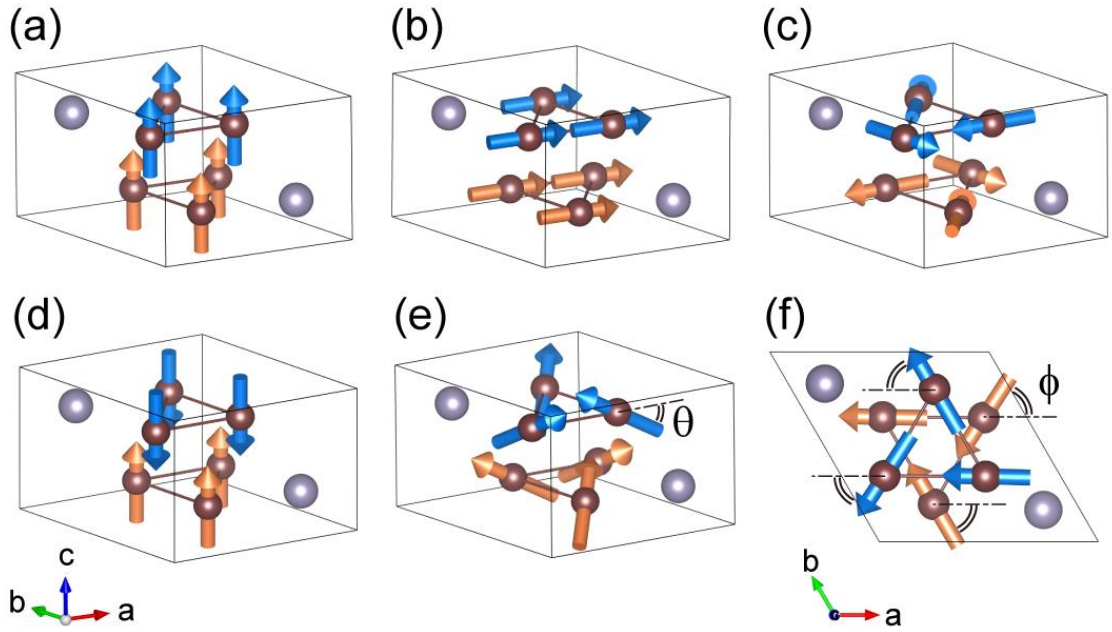

Fig. 1 (Color Online)

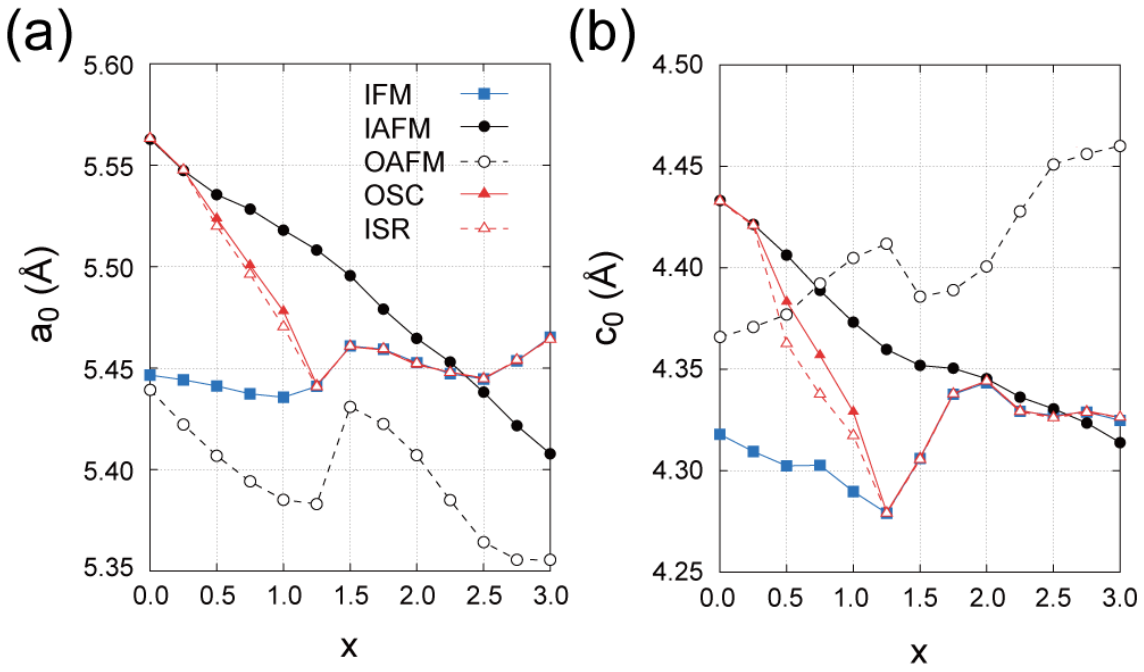

Fig. 2 (Color Online)

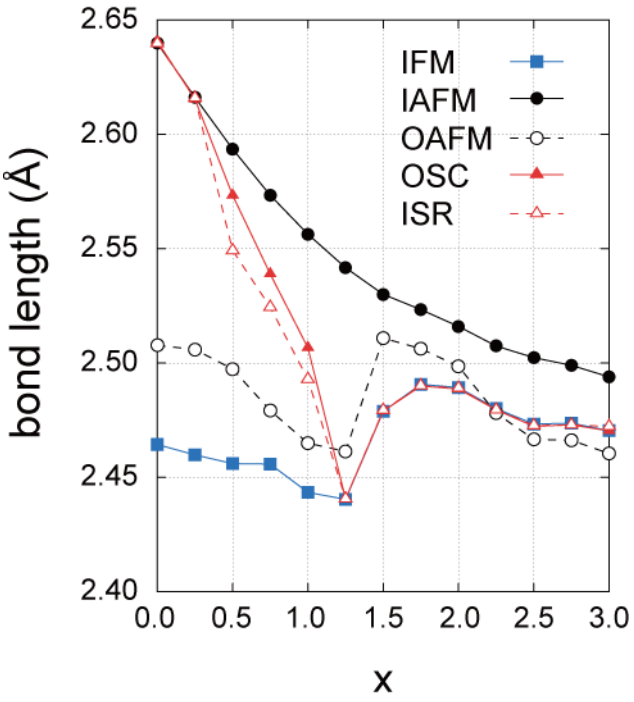

Fig. 3 (Color Online)

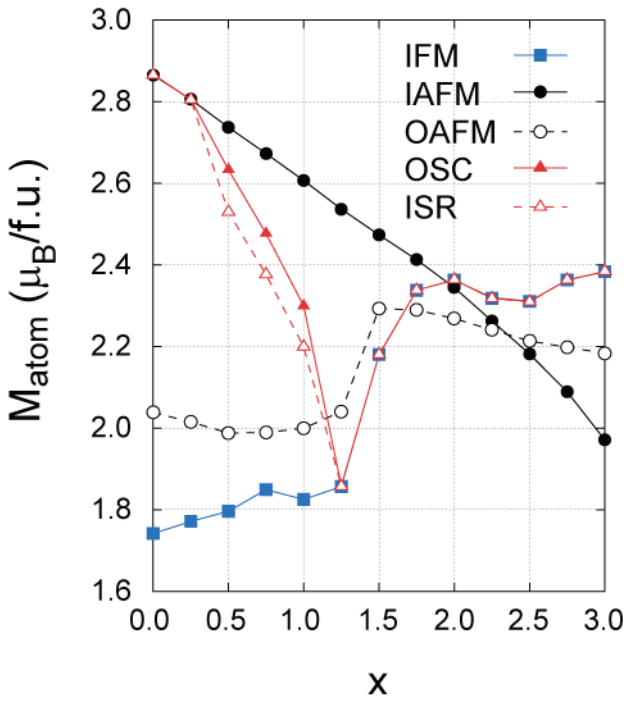

Fig. 4 (Color Online)

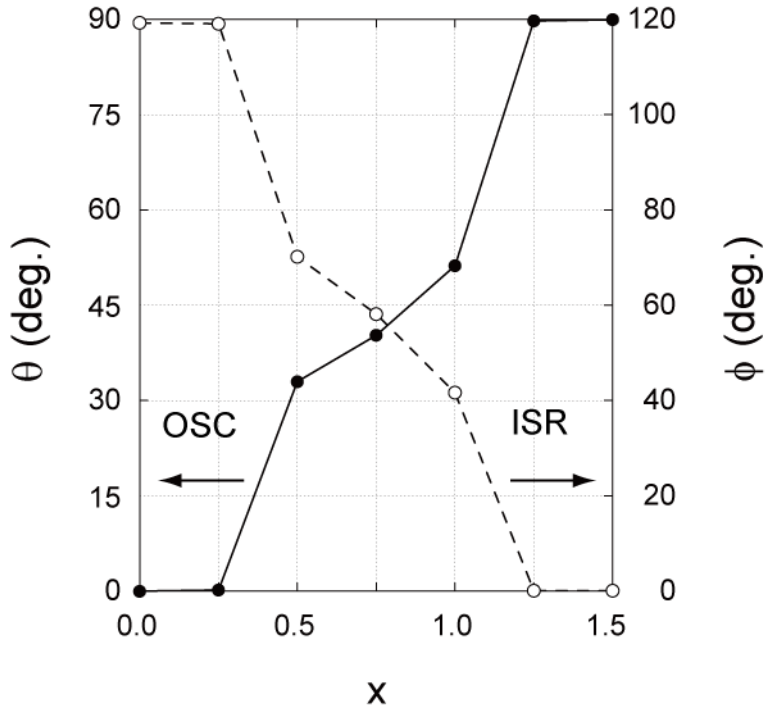
90
75
60
45
30
15
0
θ (deg.)
120
100
80
60
40
20
0
ϕ (deg.)
OSC
ISR
0.0
0.5
1.0
1.5
x

Fig. 5

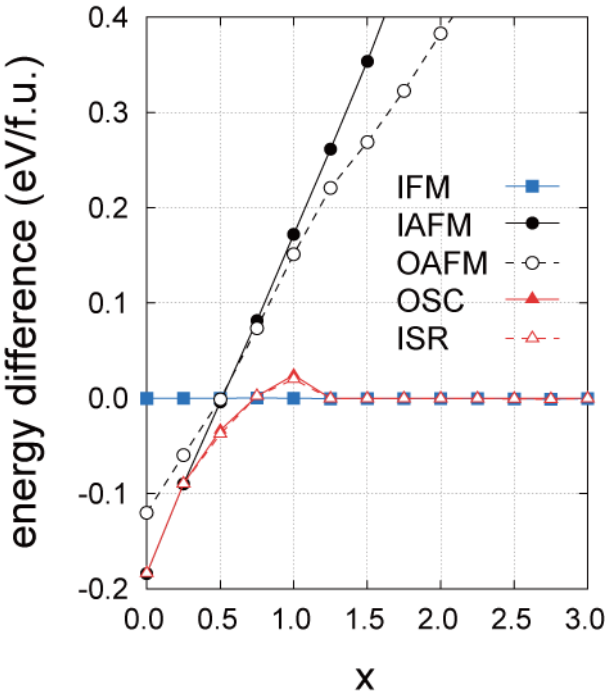

Fig. 6 (Color Online)

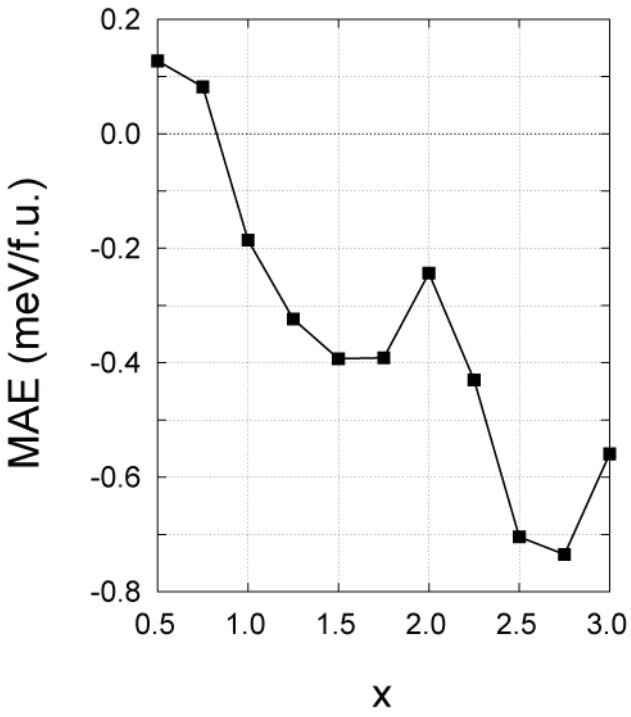

Fig. 7